JGP Journal of General Physiology

ARTICLE

Excitation–Contraction Coupling

Heart failure in mice induces a dysfunction of the sinus node associated with reduced CaMKII signaling

Jian-Bin Xue[1], Almudena Val-Blasco[1], Moran Davoodi[2], Susana Gómez[1], Yael Yaniv[2], Jean-Pierre Benitah[1], and Ana María Gómez[1]

Dysfunction of the sinoatrial node (SAN), the natural heart pacemaker, is common in heart failure (HF) patients. SAN spontaneous activity relies on various ion currents in the plasma membrane (voltage clock), but intracellular Ca^{2+} ($[Ca^{2+}]_i$) release via ryanodine receptor 2 (RYR2; Ca^{2+} clock) plays an important synergetic role. Whereas remodeling of voltage-clock components has been revealed in HF, less is known about possible alterations to the Ca^{2+} clock. Here, we analyzed $[Ca^{2+}]_i$ handling in SAN from a mouse HF model after transverse aortic constriction (TAC) and compared it with sham-operated animals. ECG data from awake animals showed slower heart rate in HF mice upon autonomic nervous system blockade, indicating intrinsic sinus node dysfunction. Confocal microscopy analyses of SAN cells within whole tissue showed slower and less frequent $[Ca^{2+}]_i$ transients in HF. This correlated with fewer and smaller spontaneous Ca^{2+} sparks in HF SAN cells, which associated with lower RYR2 protein expression level and reduced phosphorylation at the CaMKII site. Moreover, PLB phosphorylation at the CaMKII site was also decreased in HF, which could lead to reduced sarco/endoplasmic reticulum Ca^{2+}-ATPase (SERCA) function and lower sarcoplasmic reticulum Ca^{2+} content, further depressing the Ca^{2+} clock. The inhibition of CaMKII with KN93 slowed $[Ca^{2+}]_i$ transient rate in both groups, but this effect was smaller in HF SAN, consistent with less CaMKII activation. In conclusion, our data uncover that the mechanism of intrinsic pacemaker dysfunction in HF involves reduced CaMKII activation.

Introduction

Heart failure (HF), the condition where the heart cannot optimally pump blood to fulfill body needs, first during exercise and then at rest (Del Buono et al., 2019), is a serious disease with death rates >50% at 5 yr after diagnosis (Kannel, 2000). Although death among HF patients is mainly the consequence of pump failure or ventricular arrhythmias, severe bradyarrhythmias also cause sudden cardiac death in HF patients (Luu et al., 1989; Stevenson et al., 1993; Uretsky and Sheahan, 1997; Faggiano et al., 2001), suggesting sinoatrial node (SAN) dysfunction in HF (Sanders et al., 2004). Indeed, in HF patients, as well as in experimental animal models, a decrease in the intrinsic heart rate (HR) and SAN dysfunction is common (Jose and Taylor, 1969; Jose and Collison, 1970; Vatner et al., 1974; Opthof et al., 2000; Verkerk et al., 2003; Janse, 2004; Sanders et al., 2004; Du et al., 2007). Improving SAN function could potentially prevent the progression of HF (Alboni et al., 1997). In addition, chronotropic incompetence, an abnormal HR response to exercise that might reflect both an imbalance autonomic nervous system (ANS) and sinus node dysfunction per se (Zweerink et al., 2018), has been reported during the HF process (Weber et al., 1982; Higginbotham et al., 1983; Brubaker et al., 2006; Benes et al., 2013).

Although SAN dysfunction is a hallmark of HF, the mechanisms underlying HR abnormalities in HF are incompletely understood. The SAN function, the primary heart pacemaker, is accomplished by the automatic generation of action potentials. Multiple studies have shown that the spontaneous diastolic depolarization in SAN occurs because of a synergistic interaction ("coupled clock") between the voltage clock, mediated by voltage-sensitive membrane ion currents (Maltsev et al., 2006; Yaniv et al., 2015), and the Ca^{2+} clock, mediated by rhythmic spontaneous SR Ca^{2+} release and Na^+/Ca^{2+} exchanger (NCX) current activation (Lakatta and DiFrancesco, 2009). Most of the studies about understanding the mechanisms of SAN dysfunction in HF have focused on the hyperpolarization-activated, cyclic nucleotide–gated (HCN) channel subunits,

[1]Signaling and Cardiovascular Pathophysiology, UMR-S 1180, Université Paris-Saclay, INSERM, Châtenay-Malabry, France; [2]Biomedical Engineering, Technion Institute, Haifa, Israel.

Correspondence to Ana María Gómez: ana-maria.gomez@inserm.fr; Jean-Pierre Benitah: jean-pierre.benitah@inserm.fr

This work is part of a special issue on excitation–contraction coupling.

which carry the I_f current, as well as other ion channel alterations (for review, see Dobrzynski et al., 2007). However, less is known about the Ca^{2+} handling alteration in diseased SAN. The Ca^{2+} clock is initiated by spontaneous Ca^{2+} release from the SR through the Ca^{2+} release channel, the ryanodine receptor (RYR2; Lakatta et al., 2010). This Ca^{2+} is extruded by the NCX in the outer membrane, generating an inward (depolarizing) current, as it exchanges three Na^+ by each Ca^{2+} (Bogdanov et al., 2001). The propensity of RYR2 to release Ca^{2+} is modulated by the amount of Ca^{2+} stored in the SR, which also depends on sarco/endoplasmic reticulum ATPase (SERCA) activity (Lipskaia et al., 2010; Logantha et al., 2016). Moreover, spontaneous Ca^{2+} release activity also determines the degree of coupling of the clock system (Yaniv et al., 2013).

The elements involved in the Ca^{2+} clock (RYR2 and SERCA) are also expressed in ventricular cardiomyocytes, where they have a key role in excitation–contraction coupling, and they have been shown to be altered in HF (Gomez et al., 1997; Lipskaia et al., 2010). In fact, failing hearts show a decrease in SERCA function that may be due to decrease in its expression, or increase in phospholamban (PLB) expression (its natural inhibitor), or decrease in PLB phosphorylation (Chen et al., 2004; Prunier et al., 2005). This may reduce the amount of Ca^{2+} stored in the SR, which may contribute to a decrease in the amount of Ca^{2+} released to activate contraction (Eisner et al., 2017), although less efficacious excitation–contraction coupling (Gomez et al., 1997) due to transverse tubule remodeling also plays a role (Guo et al., 2013). However, the function of these Ca^{2+} handling elements, and in finding whether the Ca^{2+} clock may be involved in SAN dysfunction during HF, is largely unknown but recognized as pivotal (Dobrzynski et al., 2007).

Here, we used an experimental model of HF in the mouse by transverse aortic constriction (TAC). By Holter telemetry, we analyzed electrocardiogram (ECG) basally and after pharmacologic challenge. The HF mice showed slower HR when the ANS was blocked, and the dissected SAN showed slower spontaneous $[Ca^{2+}]_i$ transients as well as less frequent and smaller Ca^{2+} sparks. This was correlated with less activation of calcium/calmodulin-dependent protein kinase II (CaMKII) and less phosphorylation of its targets, RYR2 and PLB. Thus, our results show that in HF, Ca^{2+}/CaMKII signaling is depressed in the SAN, and this may contribute to impaired coupled clock function.

Materials and methods

HF model

Animal study was approved by the French Ministry (Ministere de l'Education Nationale, de l'Enseignement superieur et de la Recherche no. B9201901). Congestive HF was induced by TAC under anesthesia (i.p. injection of 90 mg/kg ketamine and 8 mg/kg xylazine) in C57BL/6J male mice (8 wk of age). After thoracotomy, the aortic arch was constricted between the brachiocephalic and the left carotid arteries with a thread (4.0 Prolene suture) around a blunt needle (Ø 0.385 mm; Furihata et al., 2016). The knots were tied against the needle before removing it, leaving a region of stenosis that reduced the vascular diameter. Sham-operated mice underwent the same procedure without aortic ligation and served as controls. Cardiac contractile function was assessed 8 wk after the surgery by transthoracic echocardiography, performed in a blinded fashion using an echocardiograph (Vivid 9; GE Healthcare) equipped with a 15-MHz linear transducer, under 2% isoflurane gas anesthesia in 0.8 liter/min 100% O_2. The thickness of the left ventricular (LV) anterior and posterior walls was measured in short and long axis at papillary muscle level using 2-D guided M-mode echocardiography. Measurements during systole and diastole were used to calculate parameters such as fractional shortening (FS %), ejection fraction (EF %), or LV mass, calculated using the Penn formula for rodents: LV mass (Penn) = 1.04 ([LVIDd + LVPWd + IVSd]^3 – [LVIDd]^3), where LVIDd is LV internal diameter end diastole; LVPWd is LV posterior wall dimensions; and IVSd is interventricular septal end diastole. After euthanasia under sodium pentobarbital (100 mg/kg, i.p.) anesthesia, body, heart, and lung weights were measured, as well as tibia length. Only mice with a lung weight/tibia length greater than that of sham + 2 SD were enrolled in the HF group (Vinet et al., 2008).

Table 1. **Macroscopic parameters of mice**

Parameter	Sham (n = 12)	HF (n = 12)
Body parameters		
Lung weight/tibia length	9.52 ± 0.87	15.41 ± 5.26[a]
Heart weight/tibia length	9.80 ± 0.66	16.78 ± 3.64[a]
Echocardiographic data		
FS (%)	27.62 ± 3.46	13.62 ± 3.15[a]
EF (%)	60.38 ± 5.61	33.94 ± 7.03[a]
IVSd (mm)	0.64 ± 0.10	0.65 ± 0.10
IVSs (mm)	0.92 ± 0.10	0.81 ± 0.14[a]
LVIDd (mm)	3.76 ± 0.38	4.44 ± 0.52[a]
LVIDs (mm)	2.73 ± 0.35	3.83 ± 0.48[a]
LVPWd (mm)	0.68 ± 0.14	0.78 ± 0.28
LVPWs (mm)	0.84 ± 0.10	0.86 ± 0.28
LV mass (mg)	81.60 ± 20.68	124.95 ± 65.78[a]
HR (beats/min)	470 ± 34.64	486 ± 38.10

FS, fractionnal shortening; EF, ejection fraction; IVSd, interventricular septal thickness at end-diastole; IVSs, interventricular septal thickness at end-systole; LVIDd, left ventricular internal dimension at end-diastole; LVIDs, left ventricular internal dimension at end-systole; LVPWd, left ventricular posterior wall thickness at end-diastole; LVPWs, left ventricular posterior wall thickness at end-systole. One-way ANOVA followed by Bonferroni test were used. All the values are mean ± SD.
[a]$P < 0.05$ versus sham group.

ECG recording

To monitor ECGs in awake, free-moving mice, sterilized DSI transmitters (7 ETA-F10) were subcutaneously implanted according to the manufacturer's recommendation (Cesarovic et al., 2011) after isoflurane (2.5%) inhalation anesthesia using a MINERVE workstation (0901128). The mice were placed on a warm pad (37°C), continuously receiving 1.5% isoflurane

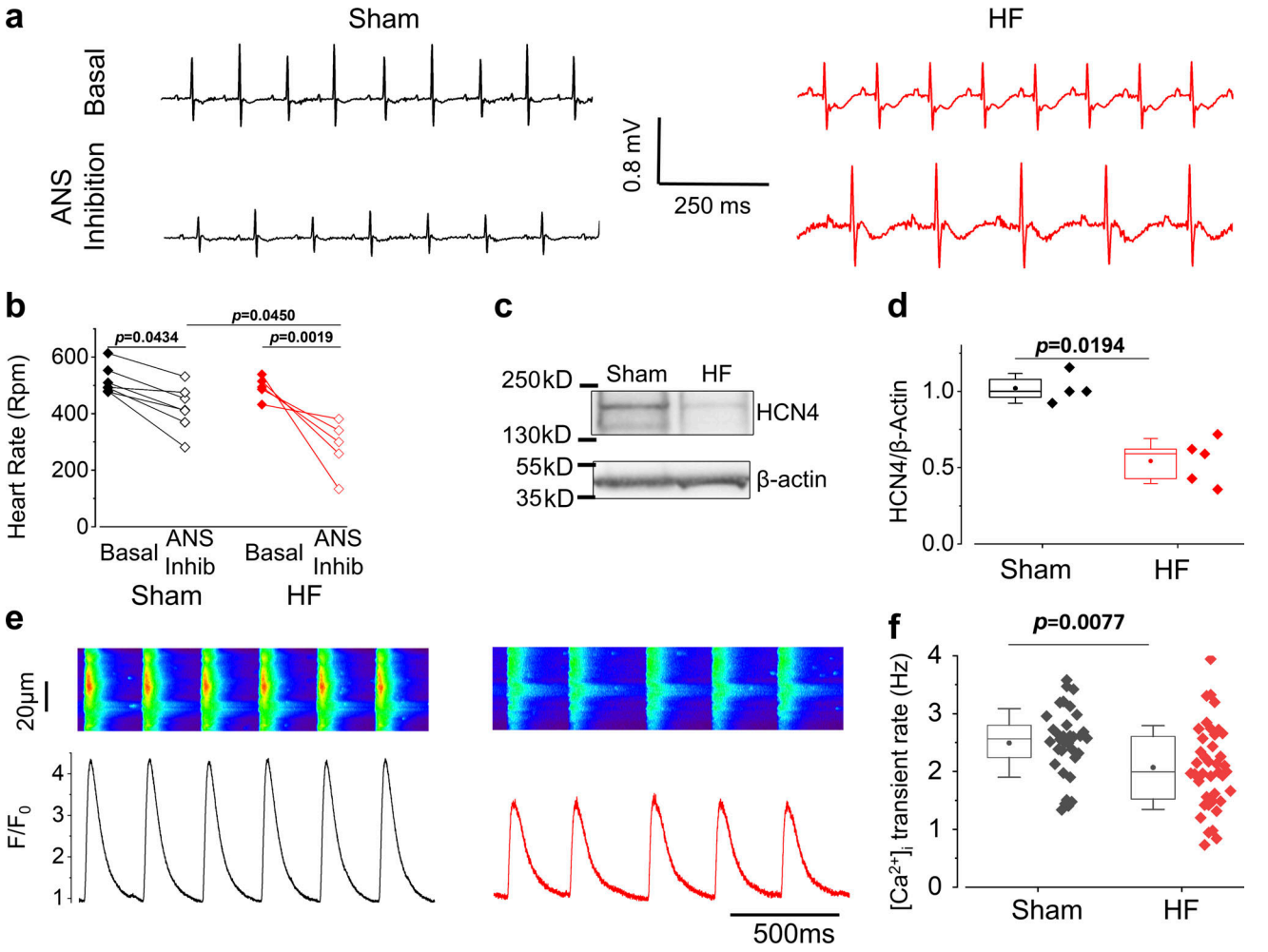

Figure 1. **The intrinsic HR and the SAN cells firing rate are lower in HF mice. (a)** Representative examples of telemetric ECG traces (daytime) under basal conditions and after atropine and propranolol injection (2 mg/kg, respectively, i.p.) from sham-operated and TAC-induced HF mice. **(b)** Quantification of HR under basal condition and upon ANS inhibition in the same mice (sham n = 7; HF n = 5). **(c and d)** Representative Western blot and quantification of HCN4 protein expression levels (sham n = 4; HF n = 5). **(e)** Examples of linescan images (0.25 ms per line) and corresponding fluorescence traces of Fluo-4 AM–loaded SAN intact tissues. **(f)** Quantification of spontaneous SAN $[Ca^{2+}]_i$ transients rate from sham and HF mice (sham, n cells = 34/N mice = 9; HF, n = 40/N = 11). Two-way repeated ANOVA followed by Bonferroni test was used in b. The P for interaction was <0.05. Nonparametric Mann–Whitney U test was used in d; in f, the data were submitted to an aligned rank transform procedure in ARTool R package, which allowed a nonparametric factorial ANOVA to be performed, taking into account the multiple observations per animal.

inhalation. After a ≥7-d recovery period, ECGs were recorded for 24 h. For sympathetic and autonomic challenges, ECGs were recorded at baseline during 20 min and at maximum effect starting from 5 min after propranolol plus atropine mixed solution (2 mg/kg each) i.p. injection. Data were collected with ECG AUTO software (EMKA Technologies). HR variability was analyzed using PhysioZoo platform (Behar et al., 2018).

In vitro intact SAN cell recording

Mice were anesthetized by sodium pentobarbital (100 mg/kg, i.p.) 8 wk after surgery. The hearts were quickly removed from the animal and placed in Tyrode solution (140 mM NaCl, 5.4 mM KCl, 1.8 mM $CaCl_2$, 1 mM $MgCl_2$, 5 mM HEPES, and 5.5 mM glucose, pH 7.4, titrated with NaOH), oxygenated to saturation, and maintained at 37°C. SAN and some surrounding atrial tissue were dissected and pinned down with the endocardial side up in homemade optical chambers bathed with Tyrode solution as previously described (Wang et al., 2017). The tissue was loaded with 30 μM fluo-4 AM (Invitrogen) during 60 min at 37°C. Images were recorded at 37°C with a resonant scanning confocal microscope, Leica SP5, equipped with a white laser fitted to 500 nm. Excitation was collected at >510 nm. The bathing solution was the same Tyrode solution supplemented with 2 μm blebbistatin to avoid movement artifacts in a temperature-controlled chamber maintained at ∼36°C. The CaMKII inhibitor, KN-93 (3 μM), or its inactive analogue, KN-92 (3 μM) was added in some experiments. 2-D and X-Time images were recorded from the primary pacemaker region, which is located in between the superior and inferior vena cava and bounded by the crista terminalis. $[Ca^{2+}]_i$ transients were recorded at spontaneous sinus rhythm and at a constant electrically imposed rhythm of 3 and 4 Hz with platinum electrodes. Ca^{2+} sparks were analyzed in the

Table 2. **Baseline ECG parameters in conscious mice**

Parameter	Sham (n = 7)		HF (n = 5)	
	Day	Night	Day	Night
RR (ms)	120 ± 10.58	108 ± 10.58[a]	123 ± 11.18	106 ± 6.71[a]
PR (ms)	38 ± 1.32	36 ± 1.06	41 ± 3.58[b]	37 ± 3.58
QRS (ms)	8.6 ± 0.45	8.7 ± 0.32	9.0 ± 0.67	9.0 ± 0.71
QT (ms)	42 ± 1.32	41 ± 1.32	51 ± 7.15[b]	47 ± 6.26

Two-way repeated ANOVA followed by Bonferroni test was used. All the values are mean ± SD.
[a]P < 0.05 versus the same group in the day period.
[b]P < 0.05 versus sham in the same period.

Table 3. **Heart-rate variability parameters in conscious sham and TAC mice during the daytime**

Parameter	Sham (n = 7)		HF (n = 5)	
	Basal	ANS inhibition	Basal	ANS inhibition
Time domain parameters				
SDNN (ms)	8.83 ± 2.51	2 ± 0.66[b]	6.89 ± 2.64	3.9 ± 2.55
RMSSD (ms)	5.03 ± 1.69	2.4 ± 0.89[b]	3.38 ± 2.21	3.95 ± 2.97
pNN5 (%)	22.5 ± 13.76	0.35 ± 0.47[b]	3.52 ± 2.68[a]	1.49 ± 2.79
Frequency parameters				
VLFreq/total (nu)	58.5 ± 2.64	48.2 ± 16.13	64.6 ± 4.25	37.9 ± 5.36[b]
LFreq normalization (nu)	66.2 ± 11.37	27.4 ± 13.76[b]	76.3 ± 5.59	53.4 ± 25.04[b,a]
HFreq normalization (nu)	33.8 ± 11.37	72.6 ± 13.76[b]	23.7 ± 5.59	46.6 ± 25.04[b,a]
LFreq/HFreq (nu)	2.79 ± 1.13	0.43 ± 0.29[b]	3.61 ± 1.18	0.82 ± 0.47

SDNN, standard deviation of the number of pairs of successive NN (Normal to Normal RR intervals); RMSSD, root mean square of the successive differences; PNN5, the proportion of the number of pairs of successive NN (R-R) intervals that differ by >5 ms divided by the total number of NN (R-R) intervals. In frequency parameters, the measures shown are the normalized power (NORM) for each band (very low frequency, VLFreq; low frequency, LFreq; and high frequency, HFreq) and the ratio of LFreq to Hfreq. Two-way repeated ANOVA followed by Bonferroni test were used. All values are mean ± SD.
[a]P < 0.05 versus sham group.
[b]P < 0.05 versus the same group under basal conditions.

diastolic period between consecutive $[Ca^{2+}]_i$ transients. The cytosolic Ca^{2+} variation was analyzed by dividing the peak fluorescence intensity (F) by the average resting fluorescence intensity (F_0). The time constant of decay (ms) was calculated by fitting the decay portion of the fluorescence trace to a monoexponential function. Analysis was made in IDL software (Exelis Visual) by homemade routines.

Isolation of SAN myocytes

For cell isolation, SAN tissue strips were transferred into a low-Ca^{2+}, low-Mg^{2+} solution containing (in mM) 140 NaCl, 5.4 KCl, 0.5 $MgCl_2$, 0.2 $CaCl_2$, 1.2 KH_2PO_4, 50 taurine, 5.5 D-glucose, 1 mg/ml BSA, and 5 HEPES-NaOH, adjusted to pH 6.9 with NaOH. Tissue was digested by Liberase TH (229 U/ml; Roche Diagnostics) and elastase (1.9 U/ml; Boehringer Mannheim) during 15–20 min at 37°C, under manual mechanical agitation. Tissue strips were then washed and transferred into a modified Kraftbruhe medium containing (in mM) 70 L-glutamic acid, 20 KCl, 80 KOH, 10 (±) D-β-OH-butyric acid, 10 KH_2PO_4, 10 taurine, 1 mg/ml BSA, and 10 HEPES-KOH, adjusted to pH 7.4 with KOH. Single SAN myocytes were then isolated by agitation in Kraftbruhe solution at 37°C. Cellular automaticity was restored by readapting the cells to a physiological extracellular Ca^{2+} concentration by addition of 10 mM NaCl and 1.8 mM $CaCl_2$ to Tyrode's solution. The final cell storage solution contained (in mM) 100 NaCl, 35 KCl, 1.3 $CaCl_2$, 0.7 $MgCl_2$, 14 L-glutamic acid, 2 (±) D-β-OH-butyric acid, 2 KH_2PO_4, 2 taurine, and 1 mg/ml BSA, pH 7.4.

To image Ca^{2+} on isolated SAN cells, they were loaded with 7 µM Fluo-4 AM for 30 min at room temperature and viewed with confocal microscopy (see above). The amplitude of the 10 mM caffeine-evoked $[Ca^{2+}]_i$ transients was used as an index of the SR Ca^{2+} load.

Western blot

SAN dissected from sham and TAC mice were lysed by Bertin homogenizer with radioimmunoprecipitation assay lysis buffer, run on 4–20% or 3–8% discontinuous gradient polyacrylamide gels depending on the molecular weight of the proteins, and transferred to nitrocellulose membranes. Nitrocellulose membranes were incubated with blocking buffer of TBS with Tween-20 (TBST; 1%) and BSA (3%). Membranes were then incubated with primary antibodies (listed in Table S1) diluted in 3% BSA TBST overnight at 4°C, followed by the secondary antibodies. Antigen complexes were visualized with iBright FL1000 (Invitrogen by Thermo Fisher Scientific) and quantified with ImageJ (National Institutes of Health).

Statistical analysis

Analyses were conducted on n cells from N mice (specified in each figure or table), as previously described (Yin et al., 2021). When conditions of parametric tests were met, statistical comparisons were performed using one- or two-way ANOVA for multiple comparisons, when appropriate. For Western blot, nonparametric Mann–Whitney U test was used. To take into account the multiple observations per animal and cells, analyses were performed with either conditional hierarchical linear mixed-effect model (lme4 R package) or with ARTool R package, for parametric and nonparametric comparisons, respectively, where the group sham or HF was the fixed effect, and animals/cells were a random effect nested in the group. Individual data points are shown, accompanied by a box (25–75% range, with median as a line, mean as a dot, and whisker SD). A value of $P < 0.05$ was considered significant.

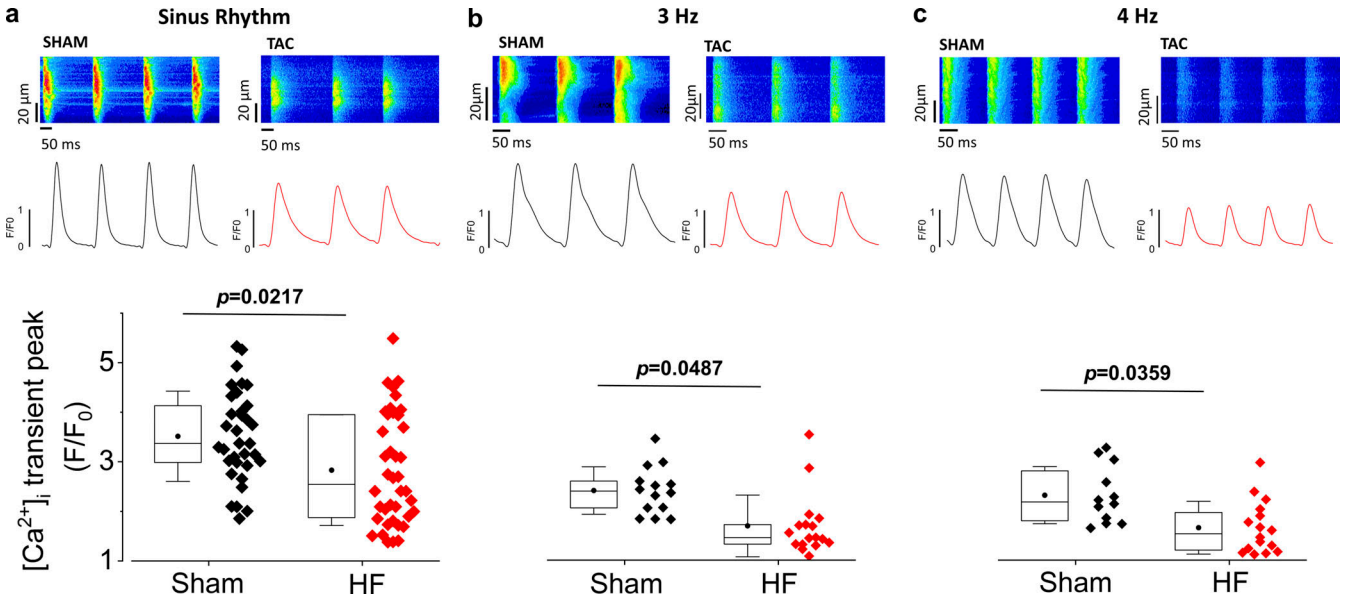

Figure 2. **The $[Ca^{2+}]_i$ transient characteristics are altered in HF SAN cells. (a–c)** Top: Representative examples of linescan images (0.25 ms per line) and corresponding fluorescence traces of Fluo-4 AM–loaded single cells from intact sham and HF SAN tissues beating spontaneously in a or electrically stimulated at 3 and 4 Hz in b and c, respectively, through a Pt electrode. Bottom: Averaged amplitude of the $[Ca^{2+}]_i$ transient measured as peak F/F_0, where F is the maximum fluorescence and F_0 is the fluorescence during diastolic periods in sinus rhythm (sham, n = 34/N = 9; HF, n = 40/N = 11), 3 Hz (Sham, n = 14/N = 3; HF, n = 17/N = 5), and 4 Hz (sham, n = 12/N = 3; HF, n = 16/N = 5). ANOVA of aligned rank transformed data was used.

Online supplemental material

Table S1 lists primary antibodies used for Western blot.

Results

TAC-induced congestive HF showed signs of SAN dysfunction

Since HF is frequently associated with abnormalities in the pacemaker system, we first analyzed ECGs in the pressure overload-induced mouse model. 8 wk after TAC, mice showed signs of congestive HF (HF group), characterized by increased heart weight/tibia length, lung weight/tibia length, and LV mass and reduced EF and FS compared with sham animals (Table 1). Holter telemetric ECG recorded during 24 h in freely moving mice, as exemplified in Fig. 1 a (upper panels), showed at baseline longer QT and PR intervals but normal RR intervals in the HF group (Table 2). However, the intrinsic HR, or the HR free of ANS influences, appeared altered (Fig. 1 a, bottom). After ANS inhibition with atropine and propanolol, the HR slowed in both animal groups, but the effect was more marked in the HF group compared with the sham group (Fig. 1 b).

To investigate the SAN and ANS contributions, we conducted analysis of the HR variability, in the time- and frequency-domain, before and after propranolol and atropine injection (Table 3). At baseline, we observed a reduction of pNN5, reflecting reduced parasympathetic activity in the HF group, whereas the total autonomic variability (SD of NN intervals [SDNN]) and vagally mediated short-term heart rate variability (HRV; RMSS) were not modified compared with the sham group. The decrease in the time-domain HRV indices following ANS blockade in the sham group was prevented in the HF group except for SDNN, implying reduced ANS function. In addition, at baseline, the HRV related to baroreceptor activity and the respiratory cycle, as gauged by low frequency (LFreq) and high frequency (HFreq), respectively, showed no change in the HF group. However, we observed an increased very low frequency (VLFreq), which denotes an enhanced SAN spectral contribution to HRV, in the HF group (Rosenberg et al., 2020). After ANS blockade, the LFreq reduction and HFreq increase observed in the HF group was less than those observed in the sham group, whereas VLFreq reduction was greater, implying reduced pacemaker function. Taken together, these results indicate that our TAC-induced congestive HF mouse model showed SAN dysfunction.

Ca^{2+} handling is depressed in SAN preparations from HF mice

SAN automaticity is dependent on synergetic interplay of voltage- and calcium-dependent mechanisms. Even if we observed a downregulation of protein expression level of HCN4 (Fig. 1, c and d) in the HF group, as consistently observed (Dobrzynski et al., 2007), little is known about rhythmic spontaneous SR Ca^{2+} release in HF SAN dysfunction. We thus recorded ex vivo the spontaneous $[Ca^{2+}]_i$ transients of Fluo 4AM–loaded SAN cells within the intact tissue (from 9 sham and 11 HF mice) by confocal microscopy (Wang et al., 2017). Fig. 1 e shows representative linescan confocal images and corresponding fluorescent traces of SAN cells from a sham and an HF mouse. The spontaneous $[Ca^{2+}]_i$ transient rate, measured between consecutive spontaneous $[Ca^{2+}]_i$ transients at their maximal upstroke, was lower in HF than in sham cells (Fig. 1 f), consistent with the decrease in intrinsic HR after ANS blockade in vivo (Fig. 1, a and b).

The Ca^{2+} handling dynamics were also altered in the HF group, as shown in Fig. 2. In HF SAN cells, the $[Ca^{2+}]_i$ transient

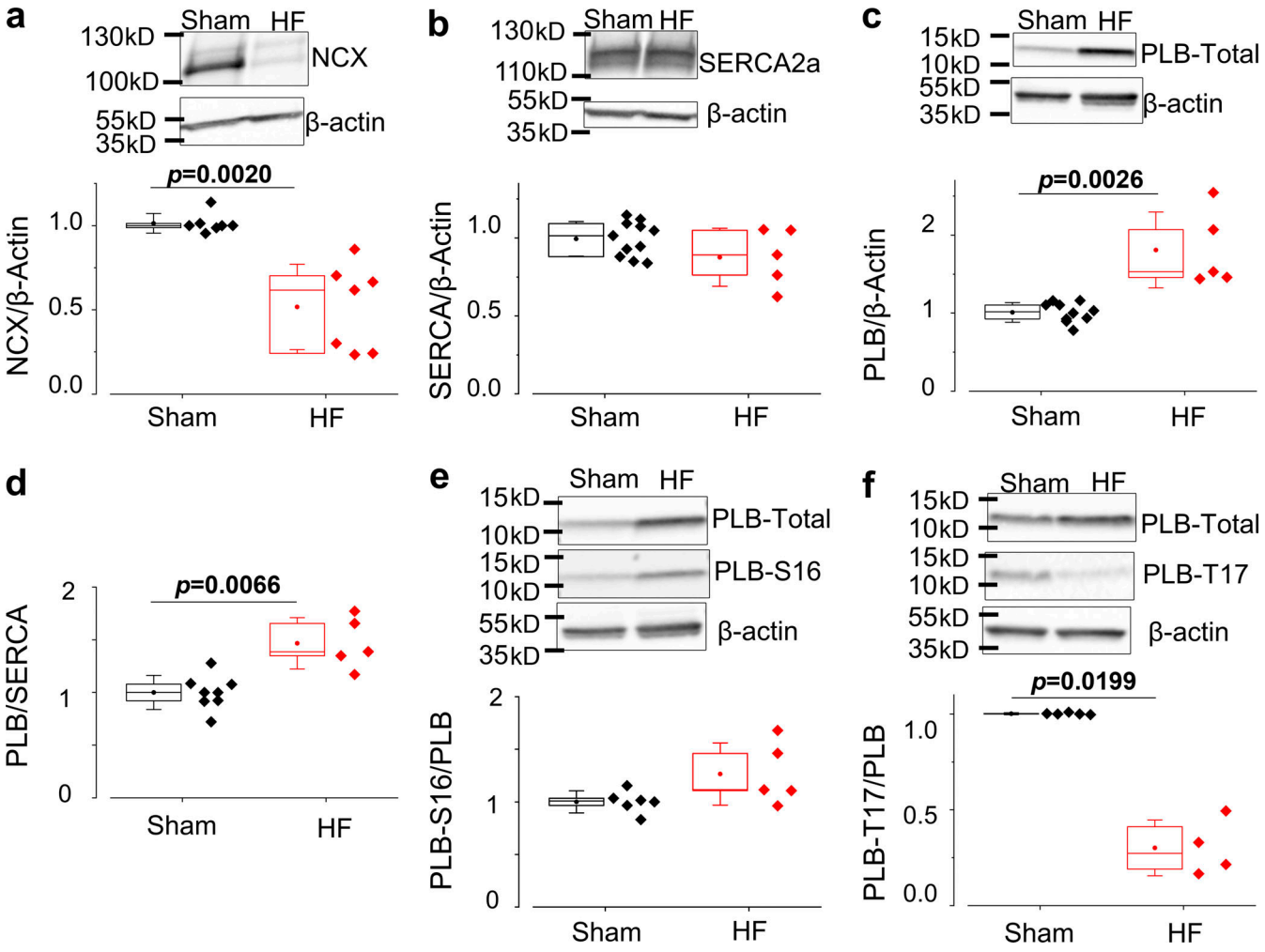

Figure 3. **NCX protein expression level decreased while total and phosphorylated PLB increased. (a–c)** Representative Western blots and quantification of protein expression levels of NCX (a), SERCA (b), and PLB (c) in SAN tissues from sham and HF mice. **(d)** Calculated PLB over SERCA ratio for each studied sample. **(e and f)** Representative Western blots and quantification of phosphorylated PLB-S16 (e) and PLB-T17 (f) normalized by PLB-total. Nonparametric Mann–Whitney *U* test was used.

peak (F/F_0) was lower (Fig. 2 a), and the decay time was longer, in HF than in sham cells (decay time constant, obtained by fitting the descending portion of the fluorescence trace to a single exponential: 58.8 ± 2.9 ms in 34 cells from 9 sham mice; 83.3 ± 4.6 ms in 40 cells from 11 HF mice; $P = 5.4 \times E^{-4}$). This reduction of $[Ca^{2+}]_i$ transient amplitude was also observed when we imposed the same rate to both groups by electrically stimulating through a Pt electrode. Fig. 2 b shows examples of Sham and HF SAN cells stimulated at 3 Hz (representative examples in top and all data in bottom) and 4 Hz (Fig. 2 c). As at sinus rhythm, $[Ca^{2+}]_i$ transients evoked at 3 and 4 Hz were also weaker in SAN cells from HF than from sham mice.

Because the $[Ca^{2+}]_i$ transient amplitude is decreased and its decay time prolonged in HF, which depends on Ca^{2+} repumping to the SR by SERCA, controlled by PLB, and extrusion by NCX, we compared their protein expression levels by Western blot. In dissected SAN tissues from sham and HF mice, the protein expression level of NCX was decreased in the HF group (Fig. 3 a). Whereas SERCA expression level was maintained (Fig. 3 b), the total PLB level was higher in the HF group than in the sham group (Fig. 3 c), leading to an increase in the ratio of PLB over SERCA (Fig. 3 d). In addition, the phosphorylation status of PLB, which relieves its inhibitory effect on SERCA, is altered. Whereas the levels of S16 PKA-dependent phosphorylation were not significantly modified (Fig. 3 e), the PLB phosphorylation levels at the T17 CaMKII site were decreased in the HF group (Fig. 3 f). Those changes on PLB might reduce SERCA function and contribute to the prolonged decay of the spontaneous SAN $[Ca^{2+}]_i$ transients in the HF group. Indeed, estimation of SR Ca^{2+} content by rapid caffeine application on isolated SAN cells showed smaller amplitude of the caffeine-evoked $[Ca^{2+}]_i$ transient in HF than in sham SAN cells (Fig. 4), indicating reduced SR Ca^{2+} load related to reduced SERCA function. As one might notice in displayed examples in Fig. 4 a, isolated SAN cells from the HF group show lower frequency, lower amplitude, and longer duration of spontaneous $[Ca^{2+}]_i$ transients as in intact SAN tissues.

To further analyze SAN Ca^{2+} dynamics, and the degree of Ca^{2+} clock coupling, we analyzed diastolic Ca^{2+} release events

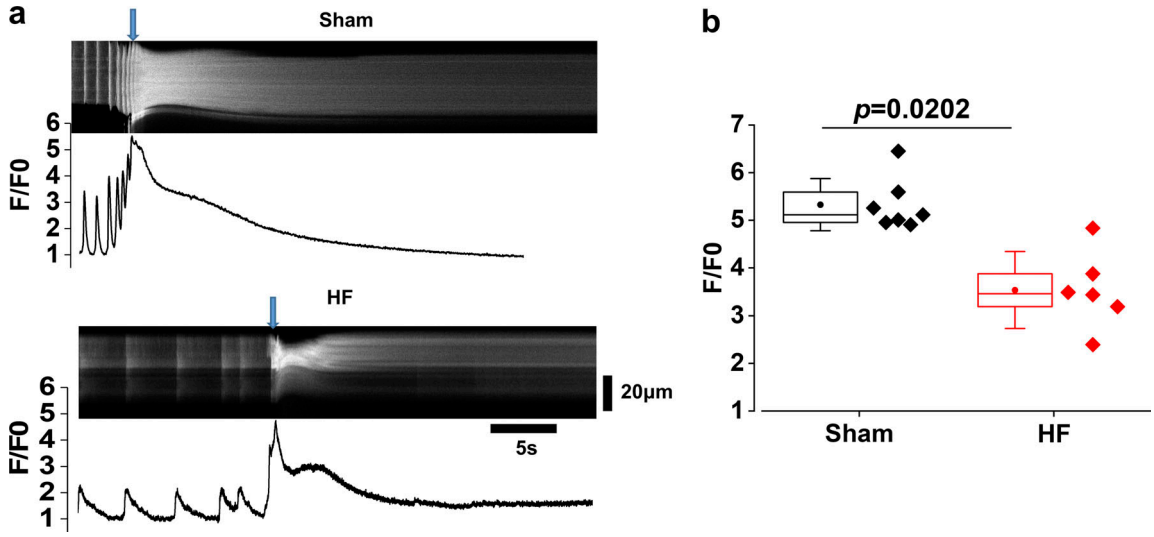

Figure 4. **SR Ca^{2+} load decreased in isolated cells of HF SAN. (a)** Linescan images (0.25 ms per line) of isolated SAN cardiomyocytes from sham and HF mice before and during caffeine perfusion; arrows indicate when caffeine was applied. **(b)** Quantification of caffeine-induced F/F_0 as an index of the SR Ca^{2+} load of SAN isolated cells of two sham (n = 7) and two HF (n = 6) mice. ANOVA of aligned rank transformed data was used.

during the diastolic phase that were observed as Ca^{2+} sparks (Fig. 5 a). We observed a lower Ca^{2+} spark frequency in the HF group (Fig. 5 b). This decrease in Ca^{2+} spark frequency was maintained when imposing a constant rate by electrically stimulating the SAN at 3 Hz (n Ca^{2+} sparks/s/100 μm: 2.00 ± 0.87 in 11 cells from 3 sham-operated mice; 0.14 ± 0.07 in 15 cells from 4 HF mice; P = 0.0174). Moreover, the Ca^{2+} spark amplitude was weaker in the HF group (Fig. 5 c), and the duration was shorter (Fig. 5 d), while the width was maintained (Fig. 5 e). Meanwhile, the time to peak of the sparks was also shorter in the HF group (Fig. 5 f), which may refer to a shorter opening time of the RYR2 channels. Moreover, the mass of the Ca^{2+} sparks, calculated as the amplitude × width × duration, was smaller in the HF cells, indicating that less Ca^{2+} is released from each Ca^{2+} spark in the HF group (Fig. 5 g).

Because the Ca^{2+} clock is referred to the late Ca^{2+} release, corresponding to the ramp of the voltage, we analyzed the amplitude of the fluorescence ramp. Fig. 5 h shows examples of the portion of $[Ca^{2+}]_i$ transient, with late local Ca^{2+} releases that is analyzed as previously at the whole $[Ca^{2+}]_i$ transient. On the bottom, the summary of the fluorescence shows the slow increase in $[Ca^{2+}]_i$ before the $[Ca^{2+}]_i$ transient upstroke. Data presented in Fig. 5 i show that the amplitude of this Ca^{2+} release was smaller in the HF group. The blowing up of the beginning of the $[Ca^{2+}]_i$ transient shows spatial heterogeneity. To better evaluate this, we calculated the fluorescence values of 5-μm subregions of the linescan images. Fig. 5 j shows linescan confocal images of single cells recorded in SAN tissues from a sham-operated mouse (top) and one HF (bottom) with the corresponding traces taken at the subregions noted on the left of each image by a short black line. It appears that the HF cell shows more heterogeneity or less synchrony. Fig. 5 k shows that on average, the variance of the time to peak of the $[Ca^{2+}]_i$ transients in the same cell at different regions is higher in HF than in the sham group.

Data presented in Fig. 5 might indicate an alteration in the RYR2. We thus evaluated RYR2 protein expression level as well as its phosphorylation status by Western blot in intact SAN tissues. We found that the total RYR2 expression was lower in SAN from HF mice compared with sham mice (Fig. 6 a). Although the RYR2 phosphorylation level at S2808, a supposed PKA site, was similar in both groups (Fig. 6 b), the phosphorylation level at S2814, a CaMKII site, was unequivocally decreased in the HF group (Fig. 6 c).

CaMKII signaling is decreased in the HF group

We were surprised to find that reduction of RYR2-S2814 CaMKII phosphorylation in SAN from HF mice, since it is classically found to be augmented in HF ventricles (Curran et al., 2010; Anderson et al., 2011; Swaminathan et al., 2012). Indeed, in the hearts of the same mice, we observed an increase of the phosphorylation level at the S2814 CaMKII site in the HF ventricles compared with sham ventricles (Fig. 6 d), indicating a different regulation during HF of CaMKII in the SAN with respect to the ventricles. We next analyzed whether this lower phosphorylation level might be related to higher phosphatase expression or less CaMKII expression and/or activity in SAN intact HF tissue. We found that the total expression level of phosphatases (Fig. 6 e) and CaMKII (Fig. 6 f) were not different between sham and HF SANs. However, the CaMKII phosphorylation level, an indicator of its activity, is reduced in the SAN from HF mice compared with sham mice (Fig. 6 f), opposite of what we observed in ventricles (Fig. 6 g), suggesting that the CaMKII signaling is differently modulated in HF SAN and ventricles.

To test whether these differences at the protein level have a functional effect, we next analyzed the selective effect on spontaneous SAN $[Ca^{2+}]_i$ transients of the CaMKII inhibitor, KN93, in SAN from both groups (Fig. 7 a). The reduction of spontaneous $[Ca^{2+}]_i$ transient rate by KN93 was smaller in HF

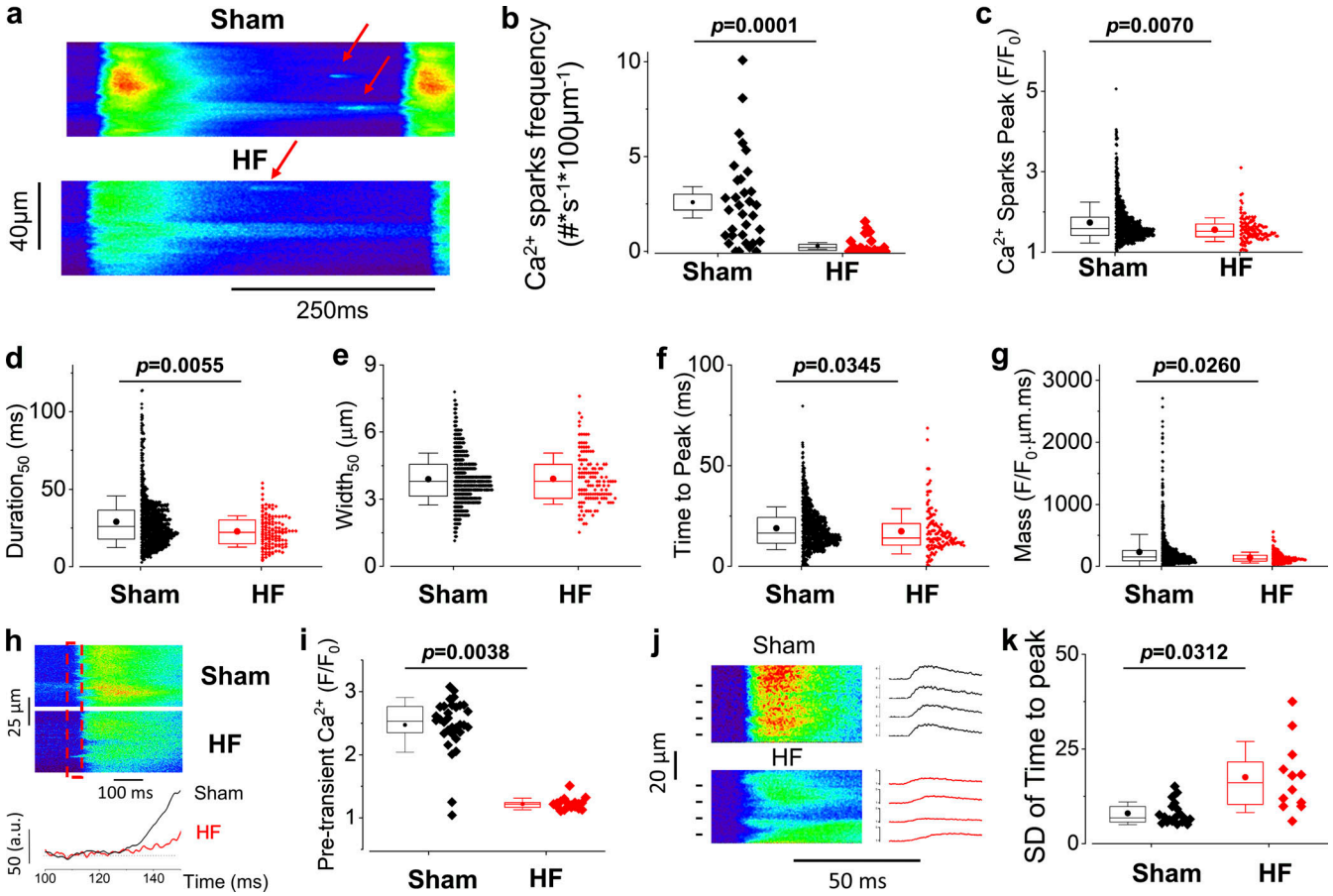

Figure 5. **HF SAN presents less frequent and smaller Ca^{2+} sparks and increased $[Ca^{2+}]_i$ transient heterogeneity. (a)** Representative linescan images (0.25 ms per line) of spontaneous beating cells from intact SAN; arrows indicate Ca^{2+} sparks. **(b)** Quantification of Ca^{2+} spark frequency (number of sparks/s/100 µm) in sham (n = 33/N = 9) and HF (n = 27/N = 9) SAN. **(c–g)** Analysis of Ca^{2+} spark characteristics (width in c, amplitude in d, half-duration time in e, time to peak in f, and mass in g) in sham (n = 992/N = 10) and HF (n = 131/N = 10) SAN. For each Ca^{2+} spark, the mass was calculated as amplitude × width × duration. **(h)** Examples of the beginning of a $[Ca^{2+}]_i$ transient in cells from a sham-operated animal (top) and an HF mouse (bottom). Below, the fluorescence traces from the region in the red box for the sham (black line) and HF (red line) images. **(i)** Quantification of the fluorescence of the fluorescence ramp (pretransient Ca^{2+}) was measured in SAN from sham (n = 32/N = 2) and HF (n = 19/N = 4) mice. **(j)** Linescan images of a $[Ca^{2+}]_i$ transient in SAN tissues from a sham (top) and HF (bottom) mouse with the corresponding traces taken at the sites noted on the right of each image. **(k)** Ca^{2+} release heterogeneity was quantified by the time to peak of the $[Ca^{2+}]_i$ transients and the SD of the time to peak for sham (n = 19/N = 3) and HF (n = 12/N = 3) mice. ANOVA of aligned rank transformed data was used.

SAN cells (Fig. 7 b), whereas its inactive derivative, KN92, failed to affect the $[Ca^{2+}]_i$ transient rate in either group (Fig. 7 c).

Discussion

Sinus node dysfunction has been observed in patients with HF (Sanders et al., 2004) as well as in different animal models. However, the underlying mechanism is still not clear. In addition to impairment of the voltage clock due to HCN4 downregulation, our study uncovers the alteration of the SAN Ca^{2+} clock under HF conditions. We observe an overall functional decrease of SAN Ca^{2+} homeostasis in HF mice, with altered $[Ca^{2+}]_i$ transient dynamics and decreased Ca^{2+} spark frequency and mass. We found that SERCA, RYR2, and NCX were downregulated, whereas PLB was upregulated, in association with a decrease of CaMKII activity. This result was the opposite in the ventricle, where CaMKII activity was increased.

Only a few and somewhat controversial studies have evaluated SAN Ca^{2+} clock function in HF. In intact dog SAN tissues after 2 wk of rapid pacing–induced HF, reduced SR Ca^{2+} release has been suggested (Shinohara et al., 2010), consistent with our results. In contrast, isolated SAN cardiomyocytes from a volume- and pressure-overload HF rabbit model showed preserved $[Ca^{2+}]_i$ transient characteristics and SR Ca^{2+} content (Verkerk et al., 2015). However, the latter study reported slower $[Ca^{2+}]_i$ transient decay due to reduced SERCA activity, as we observed in our model. Differences might be related to the HF model used and/or preparation. Nevertheless, both studies showed, at baseline or during β-adrenergic stimulation, reduced late diastolic $[Ca^{2+}]_i$ elevation in HF SAN, consistent with the decrease in Ca^{2+} spark occurrence and mass reported herein. In the SAN, Ca^{2+} sparks are considered the initiating event of the Ca^{2+} clock (Yaniv et al., 2015). Our kinetic studies on SAN Ca^{2+} sparks showed that both the peak and duration of Ca^{2+} sparks decreased in the HF group. This resulted in smaller Ca^{2+} sparks and

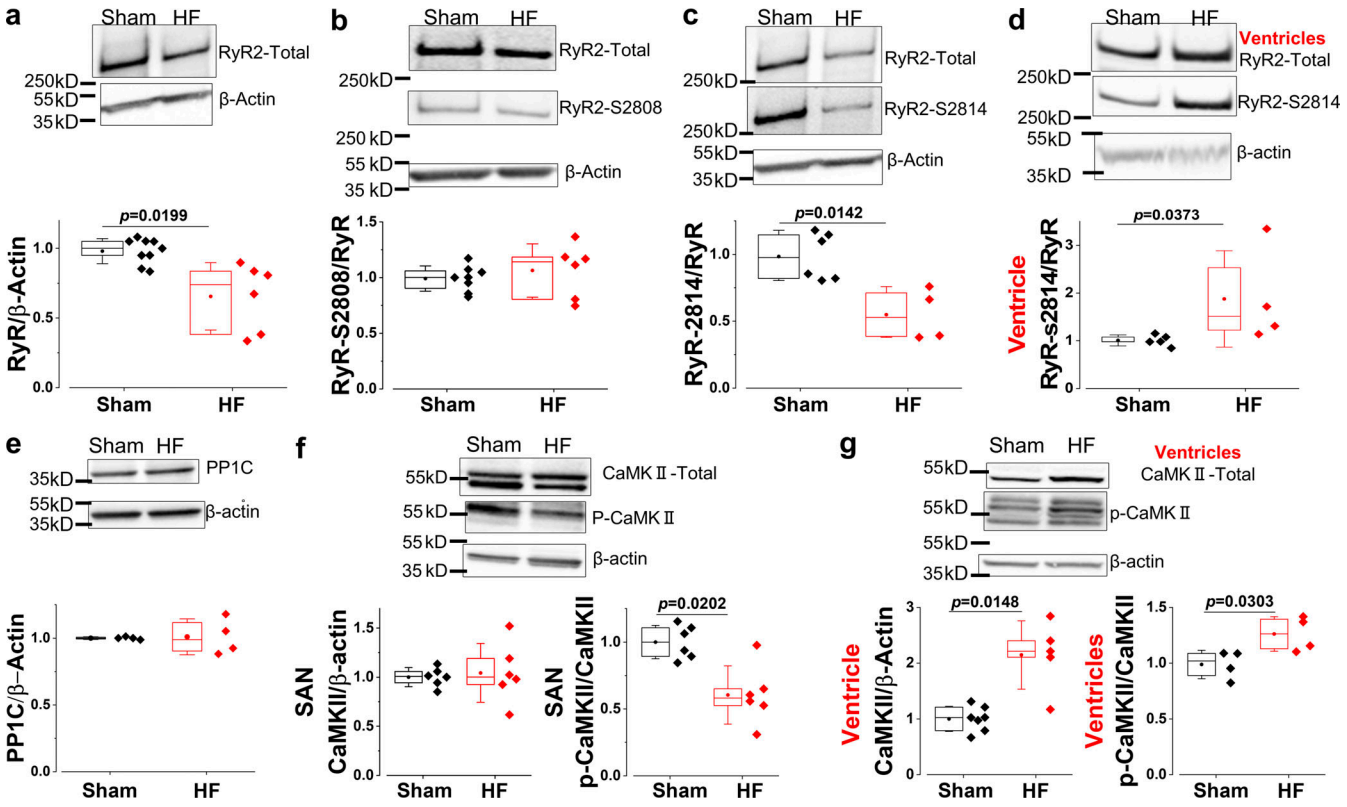

Figure 6. **RYR2 expression level and phosphorylation level decreased while CaMKII activation level decreased in HF SAN. (a–c)** Representative Western blots and quantification of RYR2-Total (a); RYR2-S2808 (b); and RYR2-S2814 (c) normalized to RYR2-total in SAN tissues from sham and HF mice. **(d)** Same as c, but in LVs from the same mice. **(e)** Representative Western blots and quantification of PP1C in SAN. **(f and g)** Representative Western blots and quantification of total and phosphorylated CaMKII (normalized by CaMKII-total) in SAN tissues (f) and ventricles (g) from sham and HF mice. The immunoblots in a, c, and f are the same as those of Fig. 3, a–c, respectively, exposed to different antibodies after stripping. Nonparametric Mann–Whitney *U* test was used.

decreased Ca^{2+} released by Ca^{2+} spark during the diastolic phase. Together with the decrease in Ca^{2+} spark frequency, it might explain the HF-induced Ca^{2+} clock malfunction. In addition, the reduction of NCX channel expression level could affect membrane depolarization and slow down the Ca^{2+} clock. Thus, our results show an impairment in the Ca^{2+} clock, which may amplify the deleterious effect of the decrease in membrane clock (Zicha et al., 2005). Together, the coupled-clock function is reduced and results in decreasing of the intrinsic sinus node automaticity, which may be compensated for on HR by the increased sympathetic activation in HF.

There are two possible reasons for the decrease in Ca^{2+} sparks. First, the decreased SR Ca^{2+} load in HF SAN, which could be related to depressed SERCA function. We found that while the SERCA protein expression level was similar in HF and sham SAN, there was an up-regulation and decreased phosphorylation level at PLB-T17 site of PLB. This may inhibit the Ca^{2+} SERCA reuptake, consistent with prolongation in the $[Ca^{2+}]_i$ transients decay time. Second, the decreased RYR2 channel expression and phosphorylation level at RYR-S2814 might further alter the regulation of the Ca^{2+} clock. Of note, both effects on PLB and RYR2 with similar protein expression of CaMKII and SERCA have been reported in SANs from rabbits with HF (Chang et al., 2017).

Our results point out an alteration of CaMKII signaling as a contributing mechanism in SAN dysfunction in HF. It has been well documented that CaMKII-dependent phosphorylation of RYR2 and PLB affect the SAN Ca^{2+} clock (Vinogradova et al., 2000; Luo and Anderson, 2013; Wu and Anderson, 2014; Li et al., 2016). Based on measurement of CaMKII autophosphorylation and phosphorylation of the CaMKII targets (RYR2-S2814 and PLB-T17), our results suggest that reduced CaMKII activation might participate in HF SAN dysfunction. Although PKA might also mediate phosphorylation of the Thr17 CaMKII site on PLB (Said et al., 2002) or phosphorylation of the Ser2814 CaMKII site on RYR2 (Ferrero et al., 2007), we did not observe a significant increase of phosphorylation of these targets at the S16 PLB or the S2808 RYR2, suggesting CaMKII specificity. Indeed, this serine/threonine kinase is initially activated by the Ca^{2+}/calmodulin complex; thus, reduction of autonomous activity of CaMKII was consistent with reduced Ca^{2+} handling. Lower CaMKII contribution to SAN activity in HF was further emphasized using CaMKII inhibitor KN93, which showed lesser effects in HF cells. Although the CaMKII role to maintain basal SAN activity is controversial in mice (Zhang et al., 2005; Wu et al., 2009), our results were consistent with a CaMKII critical role during physiopathological stress and with a basal level of activity which maintains HR. In fact, after CaMKII blockade, the HF SAN beats faster than sham SAN, indicating that in normal mouse SAN, the CaMKII basal activation is important to maintain the HR. Moreover, CaMKII dysfunction might also

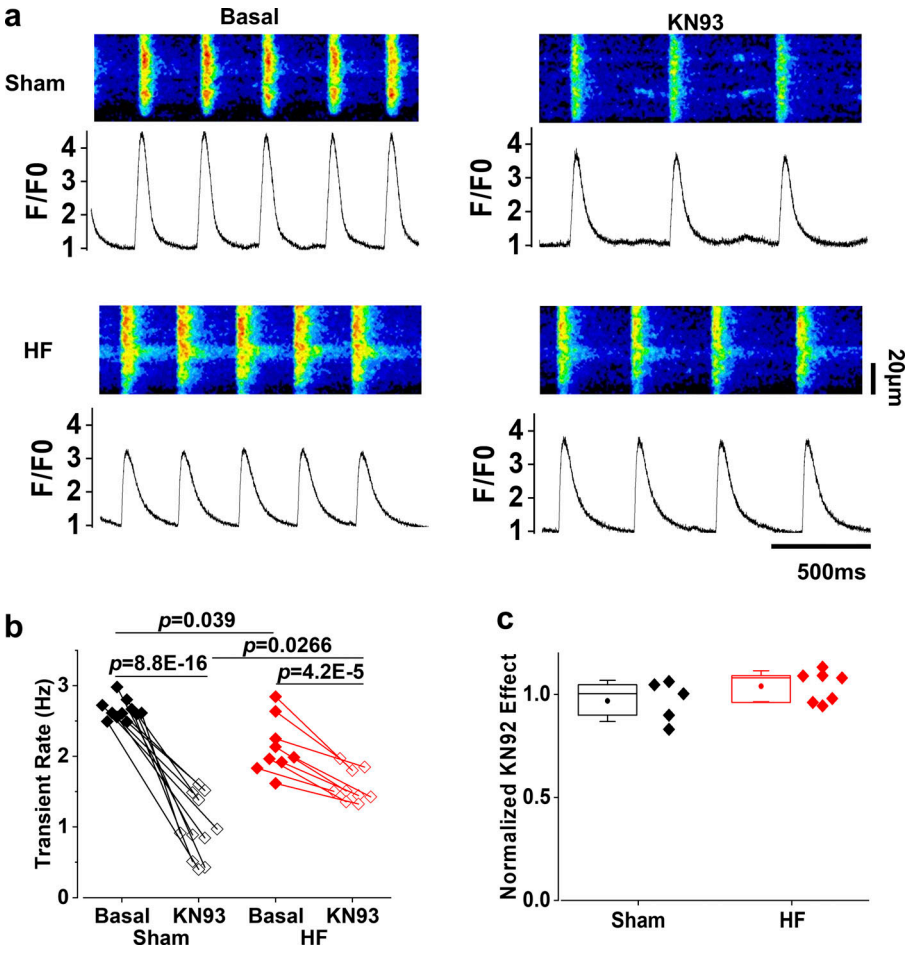

Figure 7. **CaMKII inhibition by KN93 showed less effect in HF SAN tissue. (a)** Superimposed linescan images (0.25 ms per line) and corresponding fluorescence traces, before and after 3-μM KN93 perfusion in the SAN preparation. **(b)** Calculated spontaneous $[Ca^{2+}]_i$ transient rate before and after KN93 perfusion in cells from SAN tissue of three sham (n = 11) and four HF (n = 9) mice. **(c)** Normalized effect of KN92, the inactive analogue of KN93, on the $[Ca^{2+}]_i$ transient rate in cells from SAN tissue of sham (n = 5) and HF (n = 7) mice. Each point represents the HR in the presence of KN92 normalized by the HR in the same SAN before KN92 application. The generalized linear mixed model fit by maximum likelihood (Laplace approximation) was used in b.

participate in voltage-clock perturbation in HF. The transcription factor myocyte enhancer factor 2 (MEF2) activation through CaMKII phosphorylation of histone deacetylases (HDACs) is a common end point for cardiac hypertrophic signaling pathways (Backs and Olson, 2006). Now, it is known that the HCN4 expression is in part controlled through the

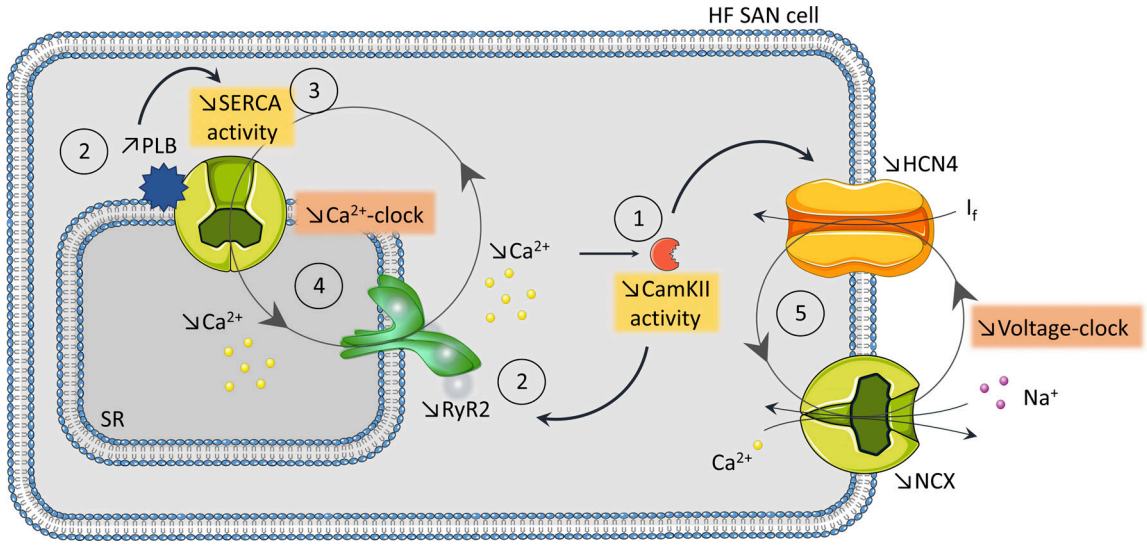

Figure 8. **Summarized schema.** In HF, SAN cells present reduced activity of CaMKII (1), leading to diminished phosphorylation in RYR2-S2814 and PLB-T17 (2), causing reduced activity of SERCA (3). In this way, the SR Ca^{2+} load is reduced and the $[Ca^{2+}]_i$ transient amplitudes are lower, also due to reduced expression of RYR2, leading to a reduction in the Ca^{2+} clock (4). Moreover, the reduction in the cytosolic $[Ca^{2+}]_i$ limits activation of the CaMKII, creating a vicious cycle by modulating the voltage clock (5), through alteration of HCN4 expression.

HDAC MEF2 system (Vedantham et al., 2013). Likewise, RYR2 promoter contains a consensus MEF2 site (Nishida et al., 1996). Altogether, this suggested a vicious circle, in which Ca^{2+} clock malfunction begets CaMKII dysfunction that in turn worsens voltage and Ca^{2+} clocks, as the mechanism responsive for SAN dysfunction in HF. This hypothesis is presented in Fig. 8. The order of the elements may vary, as the lower CaMKII activation can be the consequence of slower firing rate induced by the reduced HCN4 expression.

Further, we denoted that CaMKII was affected in opposite ways in SAN and ventricles. Likewise, HF differentially modulated HCN4 (Kuwabara et al., 2013), as well as microRNA (Yanni et al., 2020), in SAN and ventricles. This HF-related difference was also observed between SAN and ectopic pacemaker cardiomyocytes of pulmonary veins (Chan et al., 2019). The challenge is now to understand the molecular basis of these differences.

These alterations in the SAN intrinsic activity are compensated for in vivo at this stage by ANS. In fact, our analysis of HR variability presented in Table 3 shows a reduction of pNN5, reflecting reduced parasympathetic activity in the HF group.

In summary, our study, for the first time, comprehensively reveals a defect in SAN Ca^{2+} handling in TAC-induced HF mouse model, which contributes to the intrinsic pacemaker dysfunction in HF by the mechanism that includes depression in the CaMKII signaling pathway.

Acknowledgments

David A. Eisner served as editor.

The authors thank Pascale Gerbaud for advice with Western blots and Gladys Réné-Corail for administrative help.

This work was funded by INSERM (Institut National de la Santé et la Recherche Médicale), University Paris-Saclay, Agence National de la Recherche (grant ANR-19-CE-0031-01 to A.M. Gómez), Programme Hubert Curien Maimonide to A.M. Gómez and Y. Yaniv, Israel Ministry of Science to Y. Yaniv, and National Institutes of Health (grant 2R01HL055438-22 to A.M. Gómez). Jian-Bin XUE was a fellow from the Chinese Scholarship Council.

The authors declare no competing financial interests.

Author contributions: J.-B. Xue performed confocal, biochemical, and in vivo experiments and analysis; prepared figures and tables; and participated in the writing of the manuscript. A. Val-Blasco performed the confocal experiments and analysis of electrically stimulated SANs, prepared figures, and edited the manuscript. M. Davoodi analyzed the beat-to-beat variability of the electrocardiograms. S. Gómez performed TAC surgery and echocardiography measurements. Y. Yaniv supervised the beat-to-beat variability analysis and discussion, edited the manuscript, and handled funding. J.-P. Benitah wrote the manuscript, supervised the study, and performed the statistical analysis. A.M. Gómez supervised the study, wrote the manuscript, and handled funding.

Submitted: 9 February 2021
Accepted: 18 March 2022

References

Alboni, P., C. Menozzi, M. Brignole, N. Paparella, G. Gaggioli, G. Lolli, and R. Cappato. 1997. Effects of permanent pacemaker and oral theophylline in sick sinus syndrome the THEOPACE study: A randomized controlled trial. *Circulation*. 96:260–266. https://doi.org/10.1161/01.cir.96.1.260

Anderson, M.E., J.H. Brown, and D.M. Bers. 2011. CaMKII in myocardial hypertrophy and heart failure. *J. Mol. Cell. Cardiol.* 51:468–473. https://doi.org/10.1016/j.yjmcc.2011.01.012

Backs, J., and E.N. Olson. 2006. Control of cardiac growth by histone acetylation/deacetylation. *Circ. Res.* 98:15–24. https://doi.org/10.1161/01.res.0000197782.21444.8f

Behar, J.A., A.A. Rosenberg, I. Weiser-Bitoun, O. Shemla, A. Alexandrovich, E. Konyukhov, and Y. Yaniv. 2018. PhysioZoo: A novel open access platform for heart rate variability analysis of mammalian electrocardiographic data. *Front. Physiol.* 9:1390. https://doi.org/10.3389/fphys.2018.01390

Benes, J., M. Kotrc, B.A. Borlaug, K. Lefflerova, P. Jarolim, B. Bendlova, A. Jabor, J. Kautzner, and V. Melenovsky. 2013. Resting heart rate and heart rate reserve in advanced heart failure have distinct pathophysiologic correlates and prognostic impact: A prospective pilot study. *JACC Heart Fail.* 1:259–266. https://doi.org/10.1016/j.jchf.2013.03.008

Bogdanov, K.Y., T.M. Vinogradova, and E.G. Lakatta. 2001. Sinoatrial nodal cell ryanodine receptor and Na^{+}-Ca^{2+} exchanger: Molecular partners in pacemaker regulation. *Circ. Res.* 88:1254–1258. https://doi.org/10.1161/hh1201.092095

Brubaker, P.H., K.C. Joo, K.P. Stewart, B. Fray, B. Moore, and D.W. Kitzman. 2006. Chronotropic incompetence and its contribution to exercise intolerance in older heart failure patients. *J. Cardiopulm. Rehabil.* 26:86–89. https://doi.org/10.1097/00008483-200603000-00007

Cesarovic, N., P. Jirkof, A. Rettich, and M. Arras. 2011. Implantation of radiotelemetry transmitters yielding data on ECG, heart rate, core body temperature and activity in free-moving laboratory mice. *J. Vis. Exp.* 3260. https://doi.org/10.3791/3260

Chan, C.S., Y.K. Lin, Y.C. Chen, Y.Y. Lu, S.A. Chen, and Y.J. Chen. 2019. Heart failure differentially modulates natural (sinoatrial node) and ectopic (pulmonary veins) pacemakers: Mechanism and therapeutic implication for atrial fibrillation. *Int. J. Mol. Sci.* 20:3224. https://doi.org/10.3390/ijms20133224

Chang, S.L., H.L. Chuang, Y.C. Chen, Y.H. Kao, Y.K. Lin, Y.H. Yeh, S.A. Chen, and Y.J. Chen. 2017. Heart failure modulates electropharmacological characteristics of sinoatrial nodes. *Exp. Ther. Med.* 13:771–779. https://doi.org/10.3892/etm.2016.4015

Chen, Y., B. Escoubet, F. Prunier, J. Amour, W.S. Simonides, B. Vivien, C. Lenoir, M. Heimburger, C. Choqueux, B. Gellen, et al. 2004. Constitutive cardiac overexpression of sarcoplasmic/endoplasmic reticulum Ca^{2+}-ATPase delays myocardial failure after myocardial infarction in rats at a cost of increased acute arrhythmias. *Circulation*. 109:1898–1903. https://doi.org/10.1161/01.cir.0000124230.60028.42

Curran, J., K.H. Brown, D.J. Santiago, S. Pogwizd, D.M. Bers, and T.R. Shannon. 2010. Spontaneous Ca waves in ventricular myocytes from failing hearts depend on Ca^{2+}-calmodulin-dependent protein kinase II. *J. Mol. Cell. Cardiol.* 49:25–32. https://doi.org/10.1016/j.yjmcc.2010.03.013

Del Buono, M.G., R. Arena, B.A. Borlaug, S. Carbone, J.M. Canada, D.L. Kirkman, R. Garten, P. Rodriguez-Miguelez, M. Guazzi, C.J. Lavie, and A. Abbate. 2019. Exercise intolerance in patients with heart failure. JACC state-of-the-art review. *J. Am. Coll. Cardiol.* 73:2209–2225. https://doi.org/10.1016/j.jacc.2019.01.072

Dobrzynski, H., M.R. Boyett, and R.H. Anderson. 2007. New insights into pacemaker activity: Promoting understanding of sick sinus syndrome. *Circulation*. 115:1921–1932. https://doi.org/10.1161/CIRCULATIONAHA.106.616011

Du, Y., X. Huang, T. Wang, K. Han, J. Zhang, Y. Xi, G. Wu, and A. Ma. 2007. Downregulation of neuronal sodium channel subunits Nav1.1 and Nav1.6 in the sinoatrial node from volume-overloaded heart failure rat. *Pflugers Arch.* 454:451–459. https://doi.org/10.1007/s00424-007s0040216-4

Eisner, D.A., J.L. Caldwell, K. Kistamas, and A.W. Trafford. 2017. Calcium and excitation-contraction coupling in the heart. *Circ. Res.* 121:181–195. https://doi.org/10.1161/CIRCRESAHA.117.310230

Faggiano, P., A. d' Aloia, A. Gualeni, A. Gardini, and A. Giordano. 2001. Mechanisms and immediate outcome of in-hospital cardiac arrest in patients with advanced heart failure secondary to ischemic or idiopathic dilated cardiomyopathy. *Am. J. Cardiol.* 87:655–657. https://doi.org/10.1016/s0002-9149(00)01450-8

Ferrero, P., M. Said, G. Sanchez, L. Vittone, C. Valverde, P. Donoso, A. Mattiazzi, and C. Mundina-Weilenmann. 2007. Ca^{2+}/calmodulin kinase II increases ryanodine binding and Ca^{2+}-induced sarcoplasmic reticulum Ca^{2+} release kinetics during beta-adrenergic stimulation. *J. Mol. Cell Cardiol.* 43:281–291. https://doi.org/10.1016/j.yjmcc.2007.05.022

Furihata, T., S. Kinugawa, S. Takada, A. Fukushima, M. Takahashi, T. Homma, Y. Masaki, M. Tsuda, J. Matsumoto, W. Mizushima, et al. 2016. The experimental model of transition from compensated cardiac hypertrophy to failure created by transverse aortic constriction in mice. *Int. J. Cardiol. Heart Vasc.* 11:24–28. https://doi.org/10.1016/j.ijcha.2016.03.007

Gómez, A.M., H.H. Valdivia, H. Cheng, M.R. Lederer, L.F. Santana, M.B. Cannell, S.A. McCune, R.A. Altschuld, and W.J. Lederer. 1997. Defective excitation-contraction coupling in experimental cardiac hypertrophy and heart failure. *Science.* 276:800–806. https://doi.org/10.1126/science.276.5313.800

Guo, A., C. Zhang, S. Wei, B. Chen, and L.S. Song. 2013. Emerging mechanisms of T-tubule remodelling in heart failure. *Cardiovasc. Res.* 98:204–215. https://doi.org/10.1093/cvr/cvt020

Higginbotham, M.B., K.G. Morris, E.H. Conn, R.E. Coleman, and F.R. Cobb. 1983. Determinants of variable exercise performance among patients with severe left ventricular dysfunction. *Am. J. Cardiol.* 51:52–60. https://doi.org/10.1016/s0002-9149(83)80010-1

Janse, M.J. 2004. Electrophysiological changes in heart failure and their relationship to arrhythmogenesis. *Cardiovasc. Res.* 61:208–217. https://doi.org/10.1016/j.cardiores.2003.11.018

Jose, A.D., and D. Collison. 1970. The normal range and determinants of the intrinsic heart rate in man. *Cardiovasc. Res.* 4:160–167. https://doi.org/10.1093/cvr/4.2.160

Jose, A.D., and R.R. Taylor. 1969. Autonomic blockade by propranolol and atropine to study intrinsic myocardial function in man. *J. Clin. Invest.* 48:2019–2031. https://doi.org/10.1172/JCI106167

Kannel, W.B. 2000. Incidence and epidemiology of heart failure. *Heart Fail. Rev.* 5:167–173. https://doi.org/10.1023/A:1009884820941

Kuwabara, Y., K. Kuwahara, M. Takano, H. Kinoshita, Y. Arai, S. Yasuno, Y. Nakagawa, S. Igata, S. Usami, T. Minami, et al. 2013. Increased expression of HCN channels in the ventricular myocardium contributes to enhanced arrhythmicity in mouse failing hearts. *J. Am. Heart Assoc.* 2:e000150. https://doi.org/10.1161/JAHA.113.000150

Lakatta, E.G., and D. DiFrancesco. 2009. What keeps us ticking: A funny current, a calcium clock, or both? *J. Mol. Cell Cardiol.* 47:157–170. https://doi.org/10.1016/j.yjmcc.2009.03.022

Lakatta, E.G., V.A. Maltsev, and T.M. Vinogradova. 2010. A coupled SYSTEM of intracellular Ca^{2+} clocks and surface membrane voltage clocks controls the timekeeping mechanism of the heart's pacemaker. *Circ. Res.* 106:659–673. https://doi.org/10.1161/CIRCRESAHA.109.206078

Li, Y., S. Sirenko, D.R. Riordon, D. Yang, H. Spurgeon, E.G. Lakatta, and T.M. Vinogradova. 2016. CaMKII-dependent phosphorylation regulates basal cardiac pacemaker function via modulation of local Ca^{2+} releases. *Am. J. Physiol. Heart Circ. Physiol.* 311:H532–H544. https://doi.org/10.1152/ajpheart.00765.2015

Lipskaia, L., E.R. Chemaly, L. Hadri, A.M. Lompre, and R.J. Hajjar. 2010. Sarcoplasmic reticulum Ca^{2+} ATPase as a therapeutic target for heart failure. *Expert Opin. Biol. Ther.* 10:29–41. https://doi.org/10.1517/14712590903321462

Logantha, S.J.R.J., M.K. Stokke, A.J. Atkinson, S.R. Kharche, S. Parveen, Y. Saeed, I. Sjaastad, O.M. Sejersted, and H. Dobrzynski. 2016. Ca^{2+}-clock-dependent pacemaking in the sinus node is impaired in mice with a cardiac specific reduction in SERCA2 abundance. *Front. Physiol.* 7:197. https://doi.org/10.3389/fphys.2016.00197

Luo, M., and M.E. Anderson. 2013. Mechanisms of altered Ca^{2+} handling in heart failure. *Circ. Res.* 113:690–708. https://doi.org/10.1161/circresaha.113.301651

Luu, M., W.G. Stevenson, L.W. Stevenson, K. Baron, and J. Walden. 1989. Diverse mechanisms of unexpected cardiac arrest in advanced heart failure. *Circulation.* 80:1675–1680. https://doi.org/10.1161/01.cir.80.6.1675

Maltsev, V.A., T.M. Vinogradova, and E.G. Lakatta. 2006. The emergence of a general theory of the initiation and strength of the heartbeat. *J. Pharmacol. Sci.* 100:338–369. https://doi.org/10.1254/jphs.cr0060018

Nishida, K., K. Otsu, M. Hori, T. Kuzuya, and M. Tada. 1996. Cloning and characterization of the 5′-upstream regulatory region of the Ca^{2+}-release channel gene of cardiac sarcoplasmic reticulum. *Eur. J. Biochem.* 240:408–415. https://doi.org/10.1111/j.1432-1033.1996.0408h.x

Opthof, T., R. Coronel, H.M. Rademaker, J.T. Vermeulen, F.J. Wilms-Schopman, and M.J. Janse. 2000. Changes in sinus node function in a rabbit model of heart failure with ventricular arrhythmias and sudden death. *Circulation.* 101:2975–2980. https://doi.org/10.1161/01.cir.101.25.2975

Prunier, F., Y. Chen, B. Gellen, M. Heimburger, C. Choqueux, B. Escoubet, J.B. Michel, and J.J. Mercadier. 2005. Left ventricular SERCA2a gene down-regulation does not parallel ANP gene up-regulation during post-MI remodelling in rats. *Eur. J. Heart Fail.* 7:739–747. https://doi.org/10.1016/j.ejheart.2004.10.007

Rosenberg, A.A., I. Weiser-Bitoun, G.E. Billman, and Y. Yaniv. 2020. Signatures of the autonomic nervous system and the heart's pacemaker cells in canine electrocardiograms and their applications to humans. *Sci. Rep.* 10:9971. https://doi.org/10.1038/s41598-020

Said, M., C. Mundina-Weilenmann, L. Vittone, and A. Mattiazzi. 2002. The relative relevance of phosphorylation of the Thr(17) residue of phospholamban is different at different levels of beta-adrenergic stimulation. *Pflugers Arch.* 444:801–809. https://doi.org/10.1007/s00424-002s0040885-y

Sanders, P., P.M. Kistler, J.B. Morton, S.J. Spence, and J.M. Kalman. 2004. Remodeling of sinus node function in patients with congestive heart failure: Reduction in sinus node reserve. *Circulation.* 110:897–903. https://doi.org/10.1161/01.CIR.0000139336.69955.AB

Shinohara, T., H.W. Park, S. Han, M.J. Shen, M. Maruyama, D. Kim, P.S. Chen, and S.F. Lin. 2010. Ca^{2+} clock malfunction in a canine model of pacing-induced heart failure. *Am. J. Physiol. Heart Circ. Physiol.* 299:H1805–H1811. https://doi.org/10.1152/ajpheart.00723.2010

Stevenson, W.G., L.W. Stevenson, H.R. Middlekauff, and L.A. Saxon. 1993. Sudden death prevention in patients with advanced ventricular dysfunction. *Circulation.* 88:2953–2961. https://doi.org/10.1161/01.cir.88.6.2953

Swaminathan, P.D., A. Purohit, T.J. Hund, and M.E. Anderson. 2012. Calmodulin-dependent protein kinase II: Linking heart failure and arrhythmias. *Circ. Res.* 110:1661–1677. https://doi.org/10.1161/circresaha.111.243956

Uretsky, B.F., and R.G. Sheahan. 1997. Primary prevention of sudden cardiac death in heart failure: Will the solution be shocking? *J. Am. Coll. Cardiol.* 30:1589–1597. https://doi.org/10.1016/s0735-1097(97)00361-6

Vatner, S.F., C.B. Higgins, and E. Braunwald. 1974. Sympathetic and parasympathetic components of reflex tachycardia induced by hypotension in conscious dogs with and without heart failure. *Cardiovasc. Res.* 8:153–161. https://doi.org/10.1093/cvr/8.2.153

Vedantham, V., M. Evangelista, Y. Huang, and D. Srivastava. 2013. Spatiotemporal regulation of an Hcn4 enhancer defines a role for Mef2c and HDACs in cardiac electrical patterning. *Dev. Biol.* 373:149–162. https://doi.org/10.1016/j.ydbio.2012.10.017

Verkerk, A.O., M.M. van Borren, A.C. van Ginneken, and R. Wilders. 2015. Ca^{2+} cycling properties are conserved despite bradycardic effects of heart failure in sinoatrial node cells. *Front. Physiol.* 6:18. https://doi.org/10.3389/fphys.2015.00018

Verkerk, A.O., R. Wilders, R. Coronel, J.H. Ravesloot, and E.E. Verheijck. 2003. Ionic remodeling of sinoatrial node cells by heart failure. *Circulation.* 108:760–766. https://doi.org/10.1161/01.CIR.0000083719.51661.B9

Vinet, L., P. Rouet-Benzineb, X. Marniquet, N. Pellegrin, L. Mangin, L. Louedec, J.L. Samuel, and J.J. Mercadier. 2008. Chronic doxycycline exposure accelerates left ventricular hypertrophy and progression to heart failure in mice after thoracic aorta constriction. *Am. J. Physiol. Heart Circ. Physiol.* 295:H352–H360. https://doi.org/10.1152/ajpheart.01101.2007

Vinogradova, T.M., Y.Y. Zhou, K.Y. Bogdanov, D. Yang, M. Kuschel, H. Cheng, and R.P. Xiao. 2000. Sinoatrial node pacemaker activity requires Ca^{2+}/calmodulin-dependent protein kinase II activation. *Circ. Res.* 87:760–767. https://doi.org/10.1161/01.res.87.9.760

Wang, Y.Y., P. Mesirca, E. Marques-Sule, A. Zahradnikova Jr., O. Villejoubert, P. D'Ocon, C. Ruiz, D. Domingo, E. Zorio, M.E. Mangoni, et al. 2017. RyR2R420Q catecholaminergic polymorphic ventricular tachycardia mutation induces bradycardia by disturbing the coupled clock pacemaker mechanism. *JCI Insight.* 2:91872. https://doi.org/10.1172/jci.insight.91872

Weber, K.T., G.T. Kinasewitz, J.S. Janicki, and A.P. Fishman. 1982. Oxygen utilization and ventilation during exercise in patients with chronic cardiac failure. *Circulation.* 65:1213–1223. https://doi.org/10.1161/01.cir.65.6.1213

Wu, Y., and M.E. Anderson. 2014. CaMKII in sinoatrial node physiology and dysfunction. *Front. Pharmacol.* 5:48. https://doi.org/10.3389/fphar.2014.00048

Wu, Y., Z. Gao, B. Chen, O.M. Koval, M.V. Singh, X. Guan, T.J. Hund, W. Kutschke, S. Sarma, I.M. Grumbach, et al. 2009. Calmodulin kinase II is required for fight or flight sinoatrial node physiology. *Proc. Natl. Acad. Sci. USA.* 106:5972–5977. https://doi.org/10.1073/pnas.0806422106

Yaniv, Y., E.G. Lakatta, and V.A. Maltsev. 2015. From two competing oscillators to one coupled-clock pacemaker cell system. *Front. Physiol.* 6:28. https://doi.org/10.3389/fphys.2015.00028

Yaniv, Y., S. Sirenko, B.D. Ziman, H.A. Spurgeon, V.A. Maltsev, and E.G. Lakatta. 2013. New evidence for coupled clock regulation of the normal automaticity of sinoatrial nodal pacemaker cells: Bradycardic effects of ivabradine are linked to suppression of intracellular Ca^{2+} cycling. *J. Mol. Cell Cardiol.* 62:80–89. https://doi.org/10.1016/j.yjmcc.2013.04.026

Yanni, J., A. D'Souza, Y. Wang, N. Li, B.J. Hansen, S.O. Zakharkin, M. Smith, C. Hayward, B.A. Whitson, P.J. Mohler, et al. 2020. Silencing miR-370-3p rescues funny current and sinus node function in heart failure. *Sci. Rep.* 10:11279. https://doi.org/10.1038/s41598-020

Yin, L., A. Zahradnikova Jr., R. Rizzetto, S. Boncompagni, C. Rabesahala de Meritens, Y. Zhang, P. Joanne, E. Marques-Sule, Y. Aguilar-Sanchez, M. Fernandez-Tenorio, et al. 2021. Impaired binding to junctophilin-2 and nanostructural alteration in CPVT mutation. *Circ. Res.* 129:e35–e52. https://doi.org/10.1161/CIRCRESAHA.121.319094

Zhang, R., M.S. Khoo, Y. Wu, Y. Yang, C.E. Grueter, G. Ni, E.E. Price Jr., W. Thiel, S. Guatimosim, L.S. Song, et al. 2005. Calmodulin kinase II inhibition protects against structural heart disease. *Nat. Med.* 11:409–417. https://doi.org/10.1038/nm1215

Zicha, S., M. Fernandez-Velasco, G. Lonardo, N. L'Heureux, and S. Nattel. 2005. Sinus node dysfunction and hyperpolarization-activated (HCN) channel subunit remodeling in a canine heart failure model. *Cardiovasc. Res.* 66:472–481. https://doi.org/10.1016/j.cardiores.2005.02.011

Zweerink, A., A.C.J. van der Lingen, M.L. Handoko, A.C. van Rossum, and C.P. Allaart. 2018. Chronotropic incompetence in chronic heart failure. *Circ. Heart Fail.* 11:e004969. https://doi.org/10.1161/CIRCHEARTFAILURE.118.004969

Supplemental material

Provided online is Table S1. Table S1 lists primary antibodies used for Western blot.